In situ balloon-borne measurements of HNO 3 and HCl stratospheric vertical profiles influenced by polar stratospheric cloud formation during the 2005–2006 Arctic winter

A Grossel, Nathalie Huret, Valéry Catoire, Gwenaël Berthet, Jean-Baptiste Renard, Claude Robert, B Gaubicher

In situ balloon-borne measurements of HNO_3 and HCl stratospheric vertical profiles influenced by polar stratospheric cloud formation during the 2005–2006 Arctic winter

A. Grossel,[1,2] N. Huret,[1] V. Catoire,[1] G. Berthet,[1] J.-B. Renard,[1] C. Robert,[1] and B. Gaubicher[1]

Received 3 August 2009; revised 21 May 2010; accepted 14 June 2010; published 5 November 2010.

[1] Within the context of the Envisat satellite validation, the Spectromètre InfraRouge par Absorption de Lasers Embarqués (SPIRALE), balloon-borne infrared spectrometer was flown in the Arctic stratosphere (Kiruna, Sweden; 67.6°N, 21.6°E) in January 2006. In situ vertical profiles of O_3, N_2O, HNO_3, and HCl were obtained between 13 and 27.3 km. The Stratospheric and Tropospheric Aerosols Counter (STAC) was mounted on board, allowing in situ characterization of the vertical particle distribution at six values of radius between 0.2 and 1.0 μm. Complex structures were observed in both HNO_3 and HCl vertical profiles with very low values in the 20.5–22 km layer and simultaneously thin layers of clouds were observed below the HNO_3 depleted layer. We used correlations of N_2O:HNO_3 and O_3:HNO_3 to characterize these layers and a model approach to investigate the processes involved. It appears that denitrification and renitrification processes have been captured that were linked to the formation of a polar stratospheric cloud. Several tests using different nitric acid trihydrate (NAT) nucleation rates in the model were performed to obtain the best agreement between microphysical and chemical results and measurements. Best results were obtained with a nucleation rate independent of temperature.

Citation: Grossel, A., N. Huret, V. Catoire, G. Berthet, J.-B. Renard, C. Robert, and B. Gaubicher (2010), In situ balloon-borne measurements of HNO_3 and HCl stratospheric vertical profiles influenced by polar stratospheric cloud formation during the 2005–2006 Arctic winter, *J. Geophys. Res.*, *115*, D21303, doi:10.1029/2009JD012947.

1. Introduction

[2] Numerous campaigns have been conducted to study polar stratospheric clouds (PSCs) and chemistry in the polar stratosphere. PSCs are indeed involved in stratospheric ozone depletion during polar winters [*Solomon*, 1999]. PSC particles provide enhanced surfaces where heterogeneous reactions can occur, leading to the activation of chlorine species efficient for ozone depletion. During the PSC formation, particles grow by HNO_3 and H_2O uptake from the gas phase. Sedimentation of the largest particles to lower altitudes can lead to a permanent removal of HNO_3, called denitrification. As nitrogen oxides can inhibit catalytic cycles of ozone destruction in the lower stratosphere by scavenging chlorine oxide, their conversion into HNO_3 and the subsequent removal of HNO_3 prolongs the ozone depletion during spring. Our knowledge of PSCs has been improved significantly over the last two decades from combined observations by remote or in situ instruments on balloons or aircraft and from satellite data such as the THESEO 2000 campaign [*Newman et al.*, 2002]. However, questions remain about the processes leading to PSC formation, especially in the Arctic stratosphere where temperatures are usually higher than in the Antarctic.

[3] Some instruments have been developed to specifically study the condensed and frozen phases, that is, the microphysical properties of PSCs and their composition. An effort has been made to combine several instruments to undertake extensive studies of cloud particles. Nitric acid trihydrate (NAT) was proposed to be the stable solid phase of PSCs at temperatures above the threshold for ice crystal formation; this hypothesis was proven by the first in situ observation during a balloon campaign at Kiruna, Sweden on 25 January 2000 [*Voigt et al.*, 2000]. Such observations were possible due to the combination of particle counters and a mass spectrometer. Since then several studies on particle microphysics have been made using mass spectrometers, optical particles counters and backscatter sondes mounted on the same balloon gondola [*Deshler et al.*, 2003; *Larsen et al.*, 2004] or the same aircraft [*Fahey et al.*, 2001]. However, the only observation of the gas phase during these campaigns was the water vapor mixing ratio measured simultaneously by a hygrometer.

[4] Efforts have also been made to perform simultaneous measurements of particles and of gas molecules. Observa-

[1]Laboratoire de Physique et Chimie de l'Espace et de l'Environnement, CNRS, Université d'Orléans, France.
[2]Presently at Institut National de la Recherche Agronomique, Science du Sol, Centre de Recherche d'Orléans, France.

0148-0227/10/2009JD012947

tions from aircraft allow studies of PSCs due to the high number of instruments that can be used simultaneously. Aerosol samplers and NO_y chemiluminescence detectors were used during the 1999–2000 winter on board an ER-2 aircraft [*Northway et al.*, 2002] to measure both NO_y gas phase and aerosols. These observations provided insight into the vertical repartition and the characteristics of PSC particles. More recently, a broad set of instruments, including a chemiluminescence detector similar to that used by *Northway et al.* [2002], an aerosol backscatter detector, and measurements of N_2O, ClO, ClOOCl, and $ClONO_2$, were mounted onboard the M55 Geophysica aircraft in February 2003 to study simultaneously PSCs and heterogeneous reactions [*Lowe et al.*, 2006]. In contrast, the number of instruments that can be carried by a stratospheric balloon is limited; however, balloons and aircraft do not provide the same information. Aircraft observations are limited to quite low altitudes (<20 km), whereas balloons can provide vertical profiles up to 30 km and above, although for a shorter period.

[5] This work focuses on the effect of chemistry on PSCs using in situ measurements made during a polar campaign above Kiruna in January 2006 and modeling using the Microphysical and Photochemical Lagrangian Stratospheric Model of Ozone (MiPLaSMO) model [*Rivière et al.*, 2000; *Rivière et al.*, 2003]. Two in situ instruments were operated simultaneously on the same balloon gondola: the Spectromètre InfraRouge par Absorption de Lasers Embarqués (SPIRALE), an infrared tunable diode laser spectrometer dedicated to the measurement of trace gas species, and a Stratospheric and Tropospheric Aerosols Counter (STAC), an optical aerosol counter. The first part of this paper is dedicated to the description of the instruments. The second part presents the detailed analysis of HNO_3 and HCl profiles and aerosol measurements obtained simultaneously. We characterize also the vertical structure of the chemical compounds observed using N_2O:HNO_3 and O_3:HNO_3 correlations. Then, an interpretation of the measurements in terms of atmospheric processes is provided using a model approach. In this part, the goal is twofold: 1. To investigate the temperature history of the air parcels and the microphysical processes occurring before the measurements, and 2. to test different parameterizations of NAT nucleation rates and heterogeneous reactions that are already under discussion by the scientific community [*Lowe and MacKenzie*, 2008 and *Drdla et al.*, 2003].

2. Instruments

[6] Measurements were performed on 20 January 2006 above Kiruna (67.9°N, 21.1°E). The launch was made as part of an Envisat validation campaign at high latitude and during the night, from 1746 UT to 1947 UT. Simultaneous profiles of O_3, N_2O, HNO_3, and HCl mixing ratios from the SPIRALE instrument and aerosol number distribution from the STAC instrument were obtained during the balloon's ascent from 13.7 to 27.3 km height. During the descent only the STAC instrument was operating.

2.1. The SPIRALE Instrument

[7] The SPIRALE instrument is an infrared spectrometer dedicated to in situ measurements of several short- and long-lived species. It has been used previously in seven successful campaigns in the tropic, middle, and polar latitudes. SPIRALE measurements enabled us to investigate the dynamical structure [*Huret et al.*, 2006; *Engel et al.*, 2006; *Müller et al.*, 2007] and detailed chemistry [*Berthet et al.*, 2006; *Berthet et al.*, 2007; *Mébarki et al.*, 2010] of the stratosphere. This instrument was also used for validation of chemical species measured by the Odin, Envisat, ACE-SCISAT, and Aura satellites [see e.g., *Urban et al.*, 2005; *Renard et al.*, 2008; *Wang et al.*, 2007; *Wolff et al.*, 2008].

[8] A detailed description of the SPIRALE instrument and its mode of operation can be found in *Moreau et al.* [2005]. Briefly, it uses six tunable laser diodes in the mid-infrared (3–8 μm) as light sources. The spectral resolution is very high (0.0005–0.0010 cm^{-1}), allowing the detection of individual ro-vibrational lines of the species. The laser beams are injected into an open air multipass Herriott cell located between two mirrors positioned at the extremities of a telescopic mast ~3.5 m long. This mast is deployed under the gondola during the flight. Species concentrations are retrieved from direct absorption measurements, by fitting experimental spectra with spectra calculated using the HITRAN 2004 database [*Rothman et al.*, 2005]. The high frequency sampling (~1 Hz) enables measurements with a very high vertical resolution, i.e., a few meters.

[9] A 430.78 m optical path was used for the flight, with 126 reflections in the cell. In this study, we focus on species relevant to PSC investigations: Hydrogen chloride, HCl, which along with $ClONO_2$ is the major inorganic chlorine reservoir species in the stratosphere, and nitric acid, HNO_3. These two species interact directly with PSC particles. The vertical profile of HCl has been deduced from the absorption line at 2925.8967 cm^{-1} and HNO_3 from a spectral microwindow that includes numerous absorption lines between 1701.5 and 1701.8 cm^{-1}. In addition, the specific lines at 2086.0191 and 2086.4294 cm^{-1} have been used for O_3 measurements and that at 1275.4929 cm^{-1} for N_2O.

[10] Measurements of pressure (by two calibrated and temperature-regulated capacitance manometers) and temperature T (by two probes made of resistive platinum wire) on board the gondola allow conversion of the species concentrations into volume mixing ratios (VMR). Uncertainties in these parameters are negligible (<1%) relative to the other uncertainties [*Moreau et al.*, 2005]. The global uncertainties in the VMR take into account random and systematic errors. The two important sources of random error are the fluctuations of the laser background emission signal and the signal-to-noise ratio. Systematic errors originate essentially from the laser line width (an intrinsic characteristic of the diode laser) and the non-linearity of the detector (only for HNO_3). The uncertainties in spectroscopic parameters (essentially the molecular line strength and pressure broadening coefficients) associated with the mixing ratios retrievals are almost negligible. Adding quadratically the random errors and the systematic errors results in total uncertainties for HCl of 20% at an altitude of 13 km, continuously decreasing to 13% at 23 km and 7% at 27 km; for HNO_3 of 20% above 17 km (increasing up to 25% below 17 km); for O_3 of 6% above 18 km and 8% below 18 km [*Cortesi et al.*, 2007]; and for N_2O of 3% (below 26 km) [*Strong et al.*, 2008].

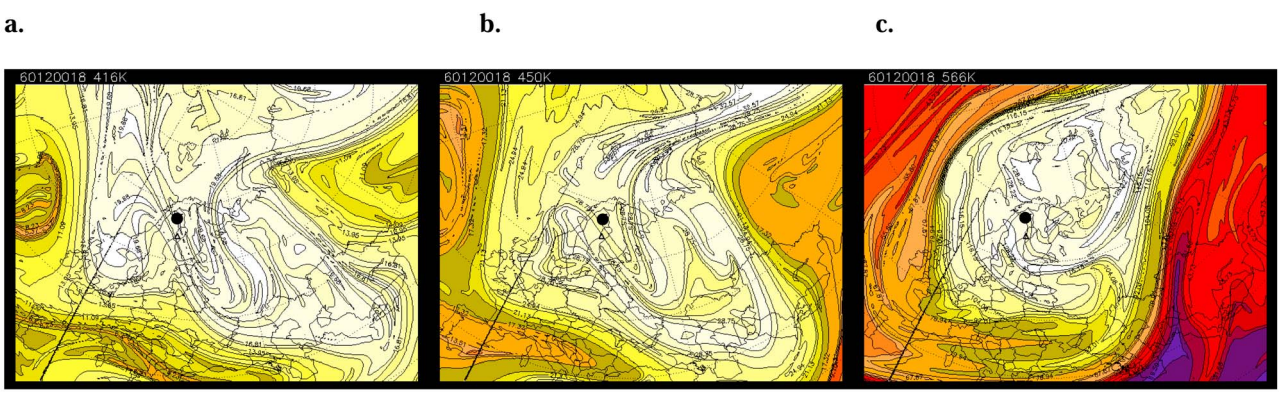

Figure 1. Potential vorticity (PV) maps calculated by the Modélisation Isentrope du transport Mésoéchelle de l'Ozone Stratosphérique par Advection (MIMOSA) model, (a) at the potential temperature 416 K (17 km altitude), (b) at 450 K (18.5 km), and (c) at 566 K (23 km). The black circle shows the payload location.

2.2. The STAC Instrument

[11] The STAC is an optical counter giving particle number densities and size distributions. It can be mounted onboard various gondolas under stratospheric balloons [*Ovarlez and Ovarlez*, 1995]. It operates under the low-pressure conditions encountered in the middle stratosphere and can detect low particle concentrations, down to about 10^{-4} particles cm^{-3} μm^{-1} [*Renard et al.*, 2005]. The particles are drawn through a light beam emitted by a laser diode at 780 nm, and scattered light is received by a photodetector at a scattering angle of 70°. The number concentrations are calculated from the count rate of the photoelectric pulses received. The sampling rate is 1 Hz. Particle radii are determined from the pulse height and are sorted into six bin sizes; assuming liquid particles composed of a common mixture of 75% H_2SO_4 and 25% H_2O with a refractive index of 1.45 [*Bemer et al.*, 1990; *Russell et al.*, 1996]. The STAC instrument was implemented onboard the SPIRALE payload. The counting uncertainty is 60% for aerosol concentrations $>10^{-3}$ cm^{-3} μm^{-1}, 20% at 10^{-2} cm^{-3} μm^{-1}, and better than 6% for concentrations >0.1 cm^{-3} μm^{-1}. The instrument cannot provide an accurate retrieval of the size distribution of solid particles having a different refractive index, including a non-zero value for the imaginary part of the index of some solid particles [*Renard et al.*, 2005]. Nevertheless, it can be used to detect qualitatively the presence of such particles, which can be less luminous than liquid droplets, provided enough light is scattered. Solid particles in clouds can be detected because they are generally larger and overall because they produce a deviation from the expected lognormal shape of liquid background aerosols [*Deshler et al.*, 2003].

3. Measurements

[12] This section presents the dynamical conditions of the measurements, the analysis of the measured HCl, HNO_3 vertical profiles, and the aerosol number distributions. Using the N_2O:HNO_3 and O_3:HNO_3 correlation points, specific layers observed are characterized in terms of denitrification and renitrification processes.

3.1. Dynamical Conditions

[13] The 2005–2006 polar winter was characterized by a relatively early and strong vortex but with a major warming starting on 21 January with a shift of the vortex toward southern latitudes, through Scandinavia to Europe [*WMO*, 2007]. At the time of the measurements, the balloon was launched inside the polar vortex [*Wolff et al.*, 2008; , *Berthet et al.*2007]. Figure 1 shows potential vorticity (PV) maps calculated by the Modélisation Isentrope du transport Mésoéchelle de l'Ozone Stratosphérique par Advection (MIMOSA) contour advection model [*Hauchecorne et al.*, 2002], based on European Centre for Medium-Range Weather Forecasts (ECMWF) meteorological data. The 416 K, 450 K, and 566 K potential temperature surfaces in the Northern Hemisphere correspond roughly to altitudes of 17, 18.5, and 23 km. At altitudes sampled by the instruments, PV fields show a well-established polar vortex centered above Northern Scandinavia.

3.2. Vertical Profile of HCl

[14] The SPIRALE HCl vertical profile exhibits very specific features (Figure 2). The dashed curve shows a mean HCl profile measured by the Atmospheric Chemistry Experiment- Fourier Transform Spectrometer (ACE-FTS) instrument for northern high latitudes [60°N–82°N, *Nassar et al.*, 2006], which can be taken as the typical state for unperturbed polar conditions. In comparison with this unperturbed profile, our HCl profile shows a strong depletion in the stratosphere at all altitudes between 24 and 17 km. This suggests clearly an activation of chlorine below 24 km due to the formation of PSC particles some time prior to the measurements. A strong gradient in the HCl mixing ratio is observed from 24 km to 22.8 km. From 21 km to 17 km the HCl mixing ratio is close to 0.7 parts per billion by volume (ppbv). The HCl variability in this layer (~15%) is close to the measurement uncertainties (see section 2.1). HCl is destroyed heterogeneously on PSC particles. Two competitive reactions

$$Cl + CH_4 \rightarrow HCl + CH_3 \quad (1)$$

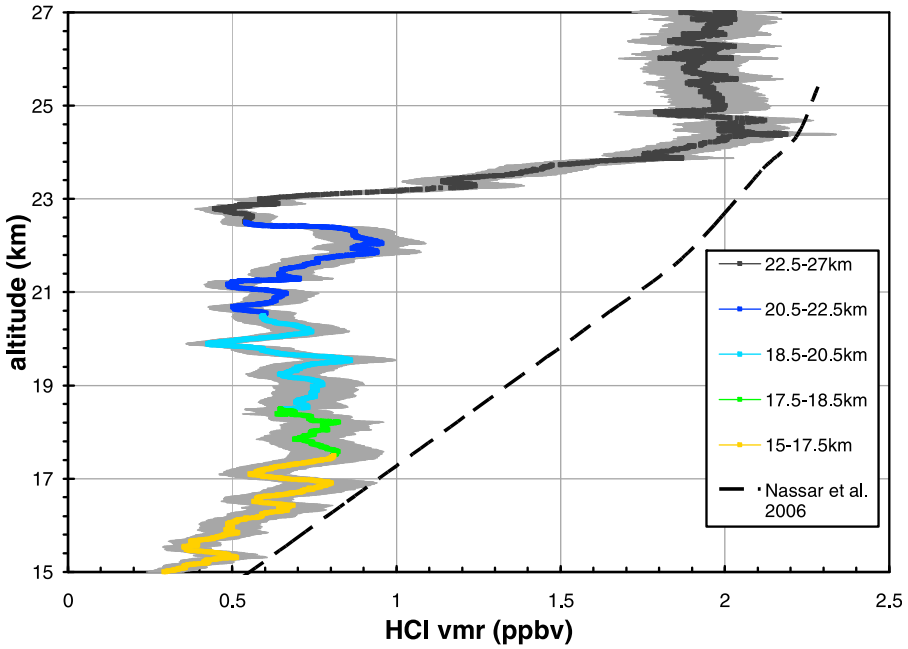

Figure 2. Vertical profile of HCl mixing ratio in ppbv and uncertainties (shaded) measured by the Spectroscopie InfraRouge par Absorption de Lasers Embarqués (SPIRALE) instrument on 20 January 2006. The colors show different altitude ranges where different processes took place (see text for details). The dashed profile is the northern high latitude profile of HCl measured by the Atmospheric Chemistry Experiment- Fourier Transform Spectrometer (ACE-FTS) instrument; mean profile 60°N–82°N, February 2004–January 2005, [*Nassar et al.*, 2006].

and

$$Cl + O_3 \rightarrow ClO + O_2 \quad (2)$$

reform the reservoir chlorine species after the onset of deactivation processes, followed by

$$ClO + NO_2 + M \rightarrow ClONO_2 + M \quad (3)$$

[15] In the Northern polar stratosphere, $ClONO_2$ mostly reforms first [*Douglass et al.*, 1995; *Wilmouth et al.*, 2006; *Santee et al.*, 2008]. This strongly depends on the geophysical conditions, which show substantial variability from one winter to another in the Arctic stratosphere. The chlorine reservoir recovery generally occurs in February or March [*Solomon*, 1999]. However, the sudden and prolonged major warming starting from mid-January 2006 [*Manney et al.*, 2008] resulted in a different situation compared to most other winters, especially in the lower and middle stratosphere. Chlorine activation and chlorine reservoir decay started as early as December 2005, but HCl and $ClONO_2$ began to reform by the end of January 2006, as can be seen from ACE-FTS and Microwave Limb Sounder (MLS) measurements [*Santee et al.*, 2008]. An analysis of their results reveals that at the time of the SPIRALE measurements the onset of HCl recovery had already occurred.

3.3. Vertical Profile of HNO_3

[16] The vertical HNO_3 profile is shown in Figure 3. The principal features of this profile are two local minima observed in the layers at 20.5–22.5 and 17.5–18.2 km. The HNO_3 vertical gradients observed above and below these minima are very strong. The HNO_3 mixing ratio is maximum at 23 km (12 ppbv) and strongly decreases down to 7 ppbv at 22.5 km. It is also important to note the two HNO_3 peaks at 20 km (10.5 ppbv) and 17 km (7.3 ppbv).

[17] When the temperature in the polar stratosphere is low enough for the formation of PSC, nitric acid is removed from the gas phase. Consequently, the depleted layer (20.5–22.5 km) is likely to be associated with a PSC formation event. Profiles showing a similar trend have already been observed during balloon campaigns, for example, by the Jet Propulsion Laboratory (JPL) MkIV interferometer [*Davies et al.*, 2006]. HNO_3 measurements are generally consistent with HCl observations in the same layer. However, in our case significant differences exist between the two SPIRALE profiles. The top of the depleted layer is characterized by a strong gradient, but not at the same altitude for both molecules. The minimum value of the HCl mixing ratio (0.5 ppbv) is observed at 23 km, exactly at the altitude of the HNO_3 maximum value. A small increase in HCl mixing ratio is observed between 21.3 and 22.4 km, where the HNO_3 mixing ratio is minimum. Finally, the local decrease in HNO_3 between 17.1 and 18.2 km does not correspond to a specific feature in the HCl profile.

3.4. N_2O:HNO_3 and O_3:HNO_3 Correlations

[18] Correlations between NO_y and long-lived tracers such as N_2O are often used to investigate denitrification [*Manney et al.*, 1999; *Kleinböhl et al.*, 2005; *Schoeberl et al.*, 2006] and renitrification [*Bregman et al.*, 1995; *Dibb et al.*, 2006] processes in the polar stratosphere. HNO_3 is the main component of NO_y in the polar vortex and the N_2O:HNO_3 correlation can thus be used to study these

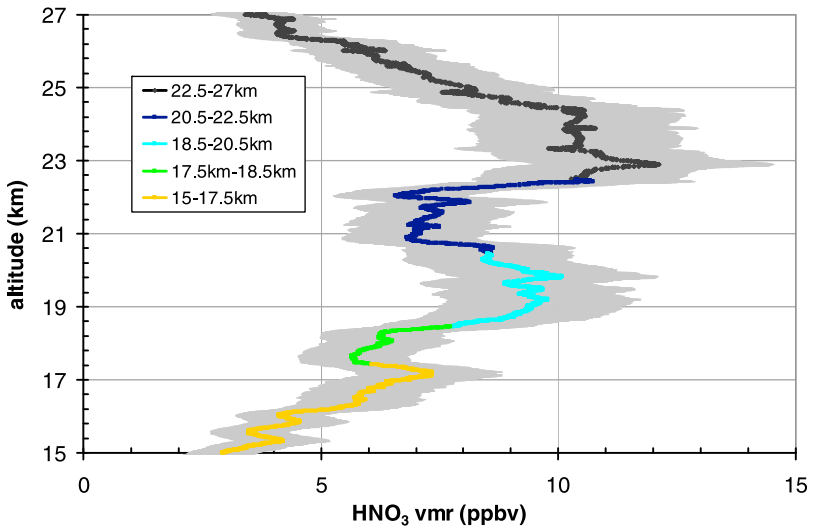

Figure 3. Vertical profile of HNO_3 mixing ratio in ppbv (color) and uncertainties (shaded) measured by the SPIRALE instrument on 20 January 2006. The colors indicate different altitude ranges.

mechanisms [*Dibb et al.*, 2006]. Figure 4a shows the N_2O:HNO_3 correlation obtained from the SPIRALE measurements at Kiruna on 20 January 2006. In agreement with the *Dibb et al.* [2006] study above North America, a linear trend between the two species is observed between 140 and 300 ppbv of N_2O, corresponding to levels below 20.5 km. The linear correlation deduced from our measurements is given by

$$[HNO_3] = 17.9 - 0.056\ [N_2O],$$

where $[N_2O]$ represents the N_2O mixing ratio in ppbv and $[HNO_3]$ the HNO_3 mixing ratio in ppbv. This slope is consistent with the lower estimation of *Dibb et al.* [2006]. For N_2O smaller than 150 ppbv, the correlation points present a specific feature typical of a denitrification layer in the altitude range 20.5–22.5 km (Figure 4a, dark blue).

[19] Additional information can also be deduced from O_3:NO_y correlation points. Typically, a linear trend is expected at high latitude [*Michelsen et al.*, 1998] but not in the cold polar vortex as NO_y species are then strongly depleted. A positive linear correlation also exists between HNO_3 and O_3 at high latitudes and deviation from this correlation enabled *Dibb et al.* [2006] to identify renitrification cases in the 9–13 km range. The O_3:HNO_3 correlation points obtained from the SPIRALE measurements are shown in Figure 4b.

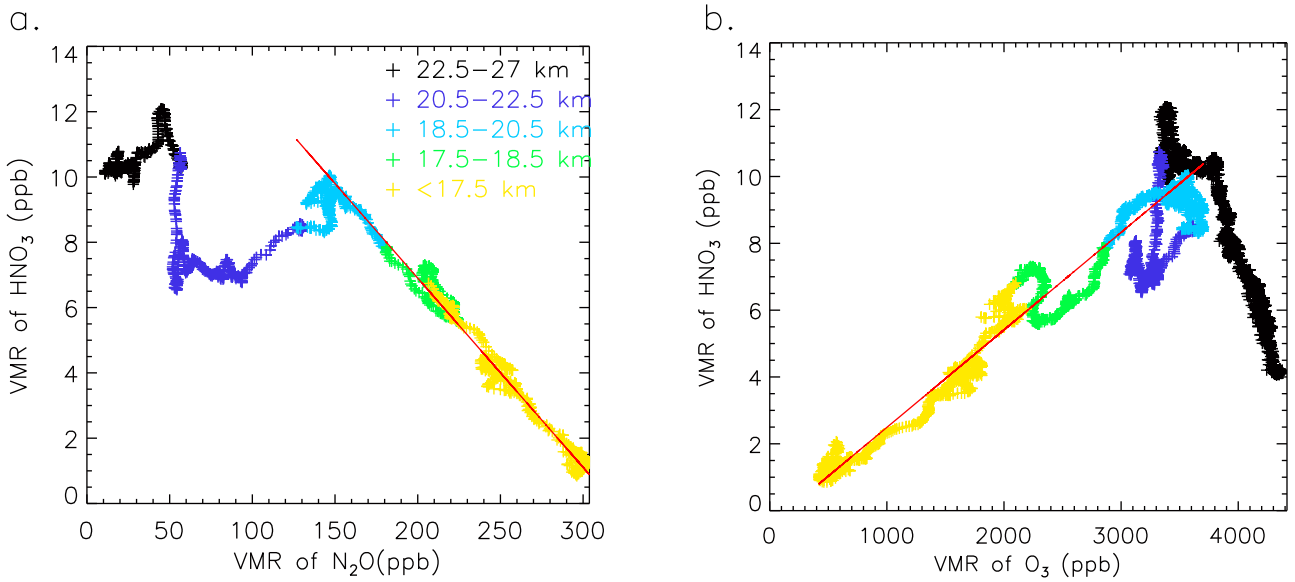

Figure 4. (a) N_2O:HNO_3 and (b) O_3:HNO_3 correlation points (ppbv for each species) obtained from SPIRALE measurements on 20 January 2006. The color scale corresponds to the altitudes range in Figures 1 and 2. The red curves show linear fits deduced from SPIRALE measurements (see text for details).

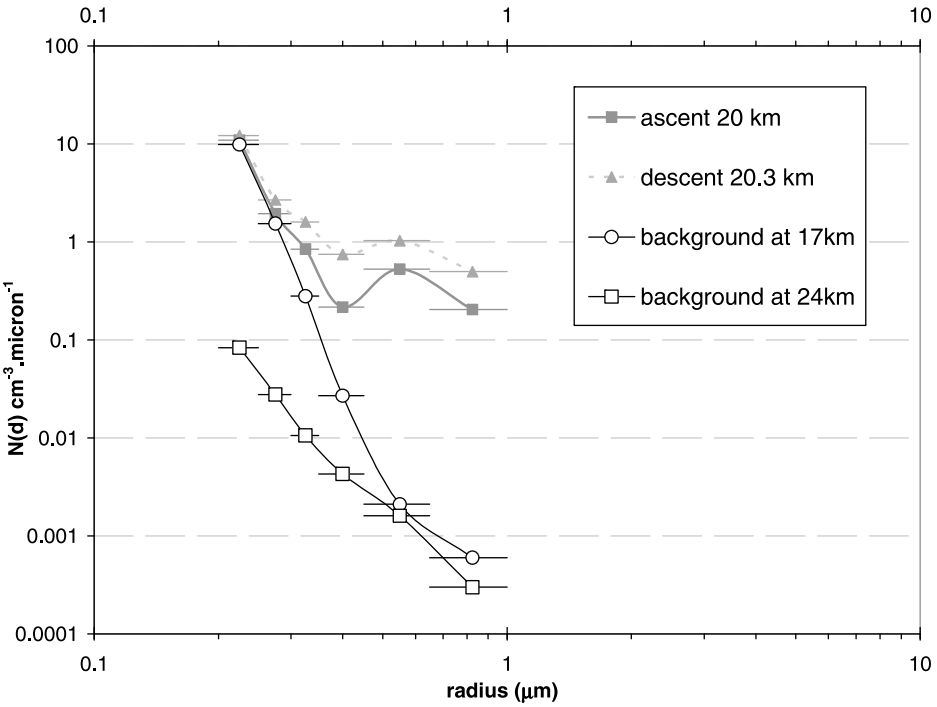

Figure 5. Number and size distribution of particles measured on 20 January 2006 during balloon ascent and descent by the Stratospheric and Tropospheric Aerosols Counter (STAC) in the SPIRALE payload. The error bars on the x axis indicate the width of each size bin. Note that it is not possible to show on this plot the largest particles (radius > 1μm) because the number size distribution cannot be calculated without an upper limit on the size interval.

A reasonably linear trend is observed up to almost 20.5 km (including most of the light blue part on the curve). The linear correlation deduced from our measurements is given by

$$[HNO_3] = -0.283 + 0.0028\ [O_3].$$

This slope is also consistent with one which can be calculated from the *Dibb et al.* [2006] study.

[20] We can characterize the denitrification and renitrification layer by the deviation of the correlation points from this linear fit. For O_3 values close to 2000 and 3500 ppbv, excesses of HNO_3 can be seen. These O_3 values correspond to altitudes close to 17 km (Figure 4b, yellow points) and 20 km (light blue points), respectively. This HNO_3 excess may be explained by considering the evaporation of PSC particles after their sedimentation from upper levels; i.e. the renitrification layers. Each renitrification layer is associated with a denitrification layer just above 20.5–22.5 km (dark blue points) and 17.5–18.5 km (green points).

[21] Note that these features can be considered real despite the large error on the HNO_3 VMR (Figure 3), which is due mostly to systematic errors and thus is constant over the whole profile. Thus, the variability of the profile is real.

3.5. Observations of Aerosols

[22] The STAC was operated during both ascent and descent. The balloon's vertical velocity during descent was very high due to operational constraints. As a consequence, the vertical resolution obtained for the STAC measurements was 5 m during the ascent and 25–35 m during the descent. Figure 5 shows the number density distribution of particles recorded by the STAC as a function of their assumed mean radius in each bin. We select two typical distributions corresponding to background aerosols having a mono-modal distribution with a large number of small size particles with radius <0.5 μm. They have been captured at 17 km and 24 km (solid curves with open circles and open squares, respectively).

[23] During the balloon's ascent, a signal was recorded for all bin sizes in a very thin (50 m) layer (Figure 5, solid shaded curve with solid squares) at 20 km. This thin layer is associated with a bimodal size distribution shape very different to the distribution shapes observed at the levels below and above. During the descent, several thin layers of particles also exhibiting such bimodal distributions were crossed from 22.5 to 18.5 km (dashed shaded curves). Notwithstanding that these descent observations were made two hours after the ascent records and separated by roughly 50 km, this result provides strong corroboration of the ascent measurements and could be interpreted as the geographically-varying presence of thin PSCs with thicknesses of a few hundred meters. The presence of solid particles has been previously observed by *Deshler et al.* [2003], with an aerosol counter showing a bimodal lognormal distribution comparable to our measurements, and by *Rivière et al.* [2000]. Because of this second and larger mode, centered on a mean radius of 0.55 μm, solid particles have probably been captured in these layers.

[24] One limitation of the STAC instrument is that it is not possible to quantify the size of particles with radii >1 μm. Note however that larger particles can in fact be detected. But as such particles would be simply classified as having a radius larger than 1 μm, it is not possible to confirm the presence of large particles of a specific size (e.g., radii between 10 and 20 μm), such as those observed with aircraft in the Arctic stratosphere in January 2000 [*Fahey et al.*, 2001] and recorded several times since [*Northway et al.*, 2002; *Larsen et al.*, 2004].

[25] Particles with a radius larger than 1μm were indeed detected (but are not shown in Figure 5). This is a further indication that there were probably solid particles present. The size distribution recorded by STAC suggests that the second mode of particles was centered on radii between 0.5 and 1 μm; keeping in mind that it is difficult to accurately infer absolute sizes for non-spherical particles using this kind of instrument [e.g., *Renard et al.*, 2005].

3.6. Measurement Analysis

[26] The vertical structure observed in both chemical and microphysical measurements is complex. In summary, the HNO_3 profile is characterized by denitrified layers (17.5–18.5 km and 20.5–22.5 km) and a renitrified layer (18.5–20.5 km) identified using correlations points (Figure 4). In the same altitude range, the HCl profile shows a weakly varying mixing ratio with low mixing ratio values probably corresponding to chlorine activation at the time of the measurements (Figure 2.). A PSC was crossed at 20 km during the ascent, whereas the descent measurements show the PSC layer having a larger extent between 22.5 and 18.5 km.

[27] The thin PSC layer at 20 km does not coincide with the altitude of the denitrified layers but does with an excess of nitric acid. This observation leads us to make the following assumption: Close to 22.5 km the formation of solid particles may have locally depleted the HNO_3 gas phase, as in the case studied by *Larsen et al.* [2002], then sedimentation occurred and a PSC was observed at 20 km. If solid particles were formed at 22.5 km and grew large enough, they would sediment, leading to the denitrification of the 20.5–22.5 km layer. At the time of measurement, the particles still present at 20 km would be evaporating and cause an excess of HNO_3 instead of a depletion.

[28] The occurrence of sedimentation processes requires particles large enough to cause irreversible denitrification. Particles with a radius larger than 10 μm will sediment more than 1 km d^{-1} [*Carslaw et al.*, 2002], whereas 1 μm particles will sediment only 0.1 km d^{-1}. Moreover, large particles can exist for longer than one day when the temperatures increase, whereas small particles evaporate after a few hours. Our measurements show the existence of particles with radii >1 μm, but provide no information on the presence or absence of particles larger than 10 μm, the so-called *NAT rocks*. The concentrations of such particles are indeed very low (of the order of 10^{-4} cm^{-3}, *Fahey et al.*, 2001].

[29] To investigate further the processes involved in the PSC formation above Kiruna on 20 January 2006, the temperature history of the air parcels encountered by SPIRALE and STAC is needed. Features observed on HCl and HNO_3 profiles can be investigated using a coupled chemical-microphysical model approach able to represent the denitrification associated with the sedimentation of PSC particles and chlorine activation mechanisms.

4. Model Interpretation

[30] In this section, we first investigate the existence of the PSC layer observed at the time of measurements using backward trajectories and measured temperature profiles. Then we use a model in order to understand the chemical and microphysical mechanisms that occurred before the measurements.

4.1. Trajectory Calculations

[31] Ensembles of backward trajectories associated with the locations of the measurements obtained during the ascent and the descent of the SPIRALE instrument have been calculated using two models. First the Hybrid Single Particle Lagrangian Integrated Trajectory (HYSPLIT; available at http://www.arl.noaa.gov/ready/hysplit4.html) model [*Draxler and Rolph*, 2003] was used with NCEP GDAS (National Centers for Environment Prediction, Global Data Assimilation System) analysis. Then isentropic trajectories were calculated using operational data from the European Centre for Medium-range Weather Forecasts (ECMWF) and the *Knudsen et al.* [2001] code. In Figure 6 we have selected three typical 6 day backward trajectories and the associated time evolution of temperature. They correspond to the levels above, inside, and below the PSC layer (556 K, i.e., 22.5 km; 481 K, i.e., 20 km; and 437 K, i.e., 18 km). The air parcels sampled during the instrument's ascent and descent have very similar origin and temperature histories. The air parcel locations are similar and in good agreement in both models.

[32] In all altitude ranges, air parcels were located inside the vortex (see section 3.1), but the trajectories show two different origins above and below 22.5 km. The air parcels arriving at and above (not shown) 22.5 km come from Greenland and stay a long time (nearly 3 days) above the Scandinavian coast whereas the air parcels between 13 and 22 km come from Siberia. It is interesting to note that differences in the air parcel origins as a function of altitude correspond exactly with the upper limit of the denitrified layer, as was checked with trajectories arriving above and below this altitude (not shown). A few days before the balloon launch, the polar vortex consisted of two joined lobes, one lobe located above Greenland and the other above Siberia.

[33] Examining the time evolution of the temperatures along the trajectories (Figure 6b) it appears that, whichever model is used, temperatures lower than 200 K were encountered by the air parcels during at least 2 days before the measurements, and for the upper trajectory the temperature remained below 200 K for more than 4 days. Temperatures obtained from the *Knudsen et al.* [2001] code with the ECMWF operational data are lower (roughly between −3 K and −4 K) than those calculated using the HYSPLIT code with the NCEP GDAS data.

[34] In addition, in Figure 7 we compare the temperature measured in situ by the SPIRALE payload and the temperature from the ECMWF analyses and NCEP GDAS data at the measurement points (end of the trajectories). From the ECMWF and NCEP GDAS analyses, it appears that the

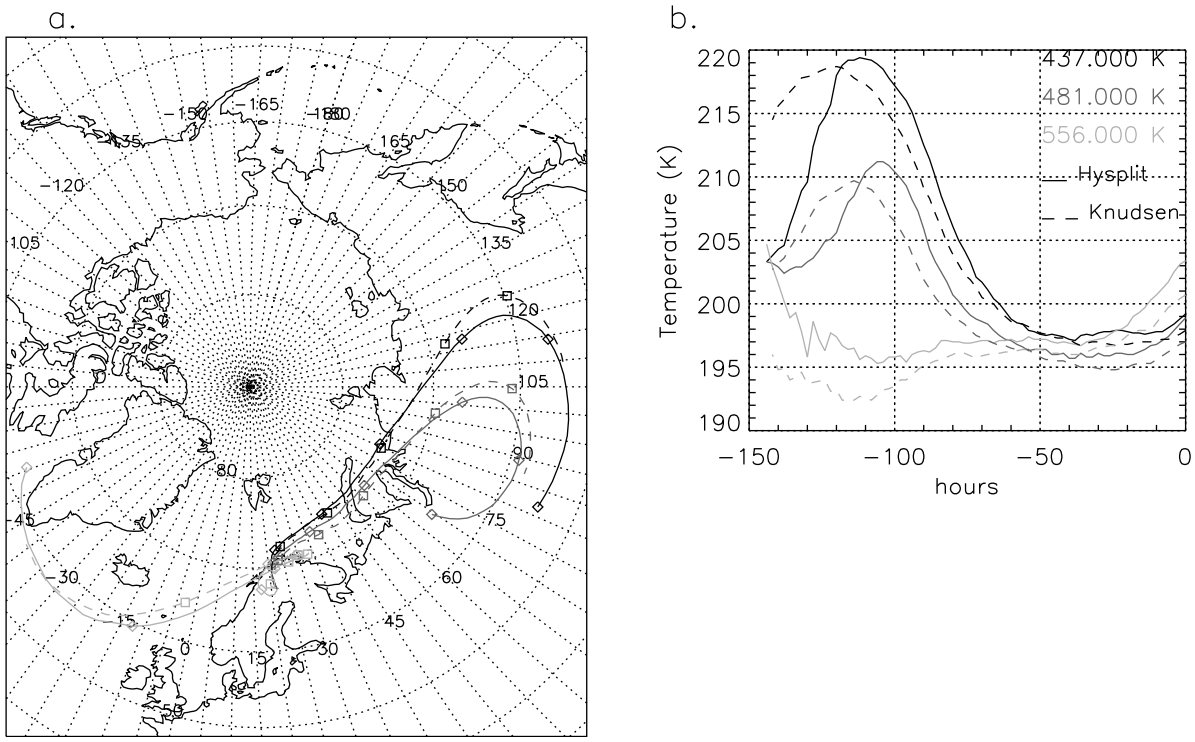

Figure 6. (a) Six day backward trajectories calculated by the Hybrid Single Particle Lagrangian Integrated Trajectory (HYSPLIT) model with the National Centers for Environment Prediction, Global Data Assimilation System (NCEP GDAS) data and with the *Knudsen et al.* [2001] code based on the operational European Centre for Medium-Range Weather Forecasts (ECMWF) data (dotted curve). The potential temperatures correspond to 437 K = 18 km (black curve), 481 K = 20 km (dark shaded curve), and 556 K = 22.5 km (light shaded curve), i.e., below, in, and above the polar stratospheric cloud (PSC) layer. (b) Temperature evolution along trajectories calculated by both models, with the same color conventions.

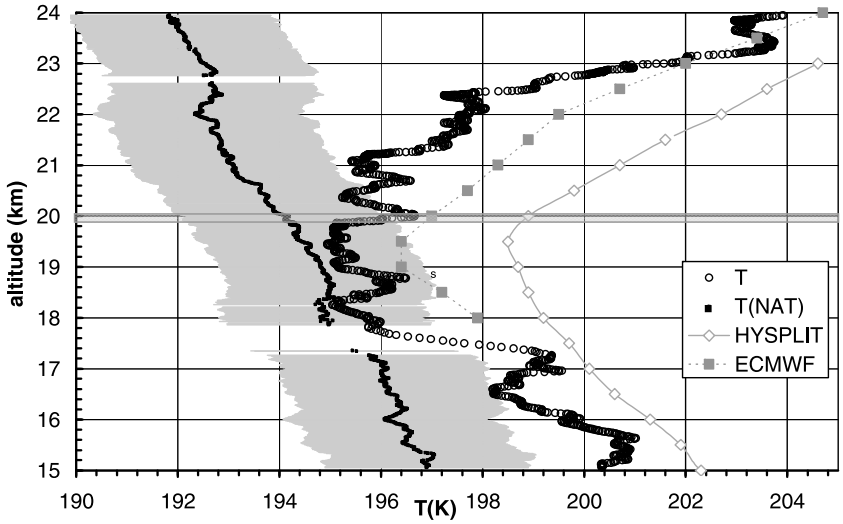

Figure 7. Vertical profile of temperature measured by SPIRALE instrument (black open circles), and calculated by the HYSPLIT model with NCEP GDAS meteorological data (shaded open diamonds), and by the model of *Knudsen et al.* [2001] with ECMWF data (shaded solid squares) at the time of measurements. The nitric acid trihydrate (NAT) equilibrium temperature (black, see text for calculation details) is shown with its uncertainties (light shaded). The shaded horizontal bar shows the PSC observation layer. Between 17 and 18 km the temperature measurements were reduced for technical reasons.

temperatures predicted are greater (+2.3 K and +4.9 K, respectively) than the in situ observations in the 20.5–22 km altitude range in the layer of interest. Disagreements in temperature between the operational ECMWF data and observations have been identified in some regions of the world: A maximum bias of 3.5 K was for example found by *Gobiet et al.* [2005] in the Antarctic vortex, and a cold bias in the tropical tropopause region was found by *Gobiet et al.* [2005] and *Knudsen et al.* [2006].

[35] Note that the meteorological conditions above Kiruna were not favorable to the propagation of mountain waves up to the stratosphere, as occurred in previous studies [*Rivière et al.*, 2000; *Brogniez et al.*, 2003], because the trajectories present a very small angle with respect to the orientation of the Scandinavian mountain range. Moreover, the wind direction was very variable from the ground to the stratosphere. Both circumstances prevent strong mountain wave activity [*Dörnbrack and Leutbecher*, 2001]. As a result, at the time of the measurements, temperatures obtained using operational ECMWF analyses are in better agreement with in situ measurements than temperatures from NCEP GDAS data, even if they are too high, by more than 2 K at some altitudes. The formation of the observed PSC is probably linked to synoptic temperature variations on a larger scale.

4.2. PSC Existence on January 20 2006

[36] The presence of a PSC should correspond to low temperatures in the polar stratosphere. The temperature measurements obtained in situ by the SPIRALE payload show that the coldest layer was encountered between 18.5 and 21 km, with a minimum value of 195 K. To investigate the PSC existence we have calculated the NAT equilibrium temperature with respect to water vapor and nitric acid content in gaseous phase using the SPIRALE HNO_3 measurements and the H_2O volume mixing ratio from the REPROBUS chemical transport model (CTM) [*Lefèvre et al.*, 1998]. Considering uncertainties of 20% in the SPIRALE HNO_3 volume mixing ratio and 20% in the REPROBUS H_2O mixing ratio [*Montoux et al.*, 2009], the NAT equilibrium temperature, T_{NAT}, is presented in Figure 7. In the layer where the PSC was detected by the STAC instrument, the temperature measured by SPIRALE is close to the NAT equilibrium temperature. These results were used previously in the study by *Wolff et al.* [2008] for the validation of HNO_3 measurements obtained with ACE-FTS satellite instrument.

4.3. Model Description

[37] The MiPLaSMO model has been used to investigate the PSC formation and its impact on chemistry through the sedimentation process. MiPLaSMO is a Lagrangian model with both microphysics calculations and a detailed chemistry scheme with 123 reactions and 10 heterogeneous reactions depending on the type of particles. This model is described in more detail by *Rivière et al.* [2000].

4.3.1. Aerosols and Chemical Species Initialization

[38] Microphysical models commonly use a lognormal distribution of background aerosols with a number density of 10 cm^{-3} [*Deshler et al.*, 2003]. *Tabazadeh et al.* [2001] used an initial number density of 15 cm^{-3}. There are very few observations and model predictions of background aerosol concentrations in the atmosphere for volcanically quiescent periods [*SPARC*, 2006] and the actual distribution is difficult to infer because few observations of very small aerosols are currently available. In this study we use a number density of 10 cm^{-3}, a mean radius of 0.087 μm and a distribution width of 1.5. This initial aerosol distribution is consistent with previous studies [*Deshler et al.*, 2003; *Tabazadeh et al.*, 2001] and in agreement with STAC observations of background particles shown on Figure 5.

[39] The initial mixing ratios of the 42 species considered in MiPLaSMO are taken from the REPROBUS three dimension (3D) CTM [*Lefèvre et al.*, 1998]. It should be noted, however, that previous studies have shown that REPROBUS, and other CTMs, strongly underestimate HCl and HNO_3 under conditions of denitrification and chlorine activation [e.g., *Ricaud et al.*, 2005; *Santee et al.*, 2008]. Therefore, we have produced monotonic initial profiles for both species by removing the denitrified, renitrified, and HCl depleted layers from the SPIRALE measured profiles and linearly interpolating across the ensuing gaps (Figures 8a and 8b). The shape and range of magnitude of the HNO_3 VMR profile obtained is consistent with the tracer-tracer correlations from the gas phase (Figure 4), which suggests no removal of HNO_3 above 23 km, a denitrified layer between 20.5 and 22.5 km and a renitrified layer below 20.5 km. When no activation occurs, the HCl mixing ratio increases with altitude in the range of the SPIRALE measurements [e.g., *Nassar et al.*, 2006] (Figures 4 and 9c). An HCl profile from the ACE-FTS at about the same date and in the closest area [*Mahieu et al.*, 2008] is also shown in Figure 8b, indicating weaker chlorine activation than the SPIRALE profile. An intermediate line (black curve in Figure 8b) between the inactivated profile and our measured profile was thus chosen as the initial profile, consistent with the mean ACE-FTS profile from the study of *Nassar et al.* [2006]. This initialization may be very approximate but more precise information is difficult to infer. Note that the choice of these initial profiles is not simple, but is consistent with satellite data and with SPIRALE measurements in layers not affected by the PSC event.

4.3.2. Solid Particles Formation

[40] Formation of NAT particles at a temperature above the ice temperature, as discussed by *Rivière et al.* [2003], can occur at low enough temperatures to form as first stage supercooled ternary solution (STS) particles (typically 3 K below the temperature T_{NAT}) which are then homogeneously nucleated to form NAT particles. Nitric acid dihydrate (NAD) particles could be taken into account but they are very quickly converted into NAT particles in the stratosphere [*Larsen et al.*, 2004]. The nucleation of NAT particles in the temperature range [T_{NAT}; T_{ice}] is not yet well understood. Both heterogeneous [*Lowe and MacKenzie*, 2008; *Drdla et al.*, 2003] and homogeneous mechanisms [*Tabazadeh et al.*, 2001] have been proposed. Laboratory studies have been carried out to evaluate the homogeneous freezing rate (hereafter J) of both NAT and NAD from droplets of binary H_2O/HNO_3 or ternary $H_2O/H_2SO_4/HNO_3$ solutions [*Bertram and Sloan*, 1998; *Salcedo et al.*, 2001]. Another open question is whether the nucleation process is initiated within droplets or if it is a surface-based process as proposed by *Tabazadeh et al.* [2002]. This last assumption leads to much higher nucleation rates but may lead to overestimation as shown by *Knopf et al.* [2002]. To successfully explain MIPAS-B instrument measurements, the J value

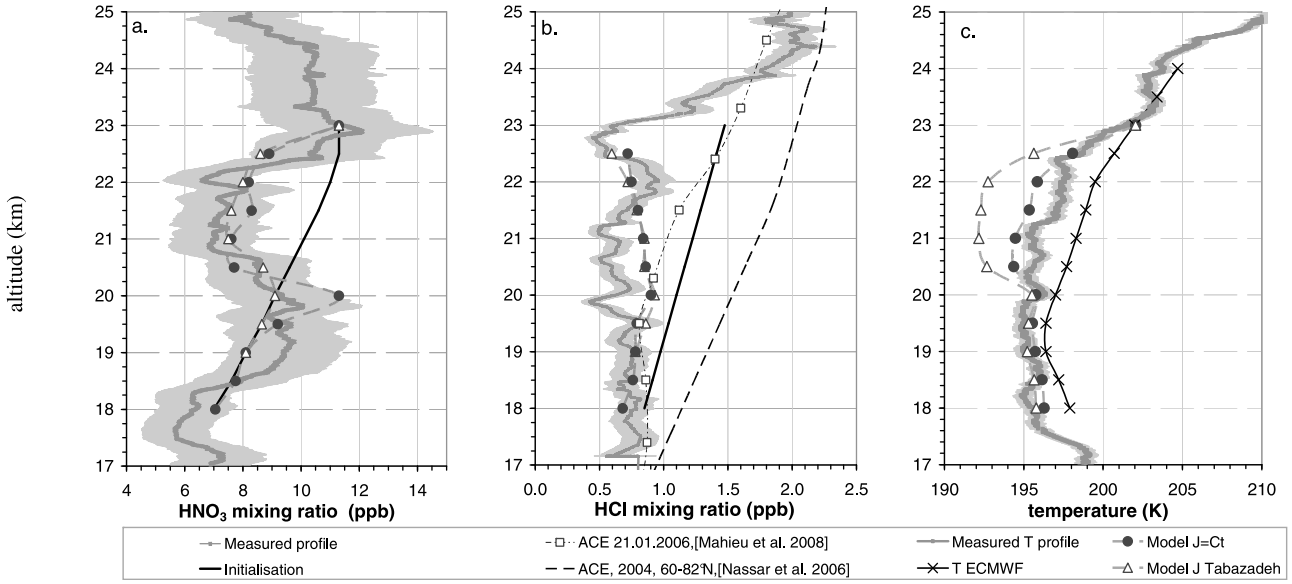

Figure 8. Comparisons between measured (shaded with uncertainties in light shading) and modeled profiles (dashed with triangles for the model results using the parameterization of [*Tabazadeh et al.* 2002] and solid circles for the parameterization using a constant nucleation rate ($J = 10^7$ cm^{-3} s^{-1}). (a) The HNO_3 profile. The black curve is the initial profile. (b) The HCl profile. Profiles from the ACE-FTS instrument are also shown. The dashed curve shows the mean Northern high latitude HCl profile for 2004 [*Nassar et al.* 2006]. The dashed dotted profile with open squares shows a profile at a close position on 21 January 2006 [*Mahieu et al.*, 2008]). (c) Temperature profile. The black profile with × symbols indicates the ECMWF temperatures. The model profiles are the assumed temperatures at the end of trajectories.

was reduced by a factor of 20 in [*Larsen et al.* 2004]. New laboratory studies were carried out by [*Stetzer et al.* 2006] on NAD formation between 192 K and 197 K, reproducing as much as possible stratospheric conditions, to find answers to the ongoing debate. They proposed a new parameterization of the activation energy [*Mölher et al.*, 2006], leading to much weaker J than the *Tabazadeh et al.* [2002] study.

[41] No definitive conclusion has yet been reached. Model studies often use simple nucleation schemes without temperature dependence [*Carslaw et al.*, 2002; *Drdla et al.*, 2003, and *Grooß et al.*, 2005]. An extensive study of the 1999–2000 winter based on measurements made during the SAGE III Ozone Loss and Validation Experiment (SOLVE) campaign by aircraft instruments (both microphysics and chemistry) was made by *Drdla et al.* [2003] and *Drdla and Browell* [2004] with a complete comparison of the different parameterizations of nucleation rates. The simplest model, ignoring the temperature dependence of nucleation rates, gave the best agreement with observations. None of the more detailed parameterizations were able to reproduce the observations [*Drdla and Browell*, 2004].

[42] In this study we have performed sensitivity tests on the nucleation rates with volume-based parameterization based on the *Salcedo et al.* [2001] study, the surface-based parameterization of *Tabazadeh et al.* [2002], the *Möhler et al.* [2006] parameterization, and on constant J values between 10^3 and 10^9 cm^{-3} s^{-1} in order to predict both microphysical and chemical in situ observations.

4.3.3. Sedimentation

[43] Sedimentation of PSC particles was included in the model. We made the calculations with a vertical step of 500 m on trajectories ending at measurement points. The spatial and temporal coincidence between air parcels was checked and, in the case of coincidence, the particles can sediment to the lower level. The air parcels traversed by the balloon above Kiruna have very distinct origins. Above 22.5 km they come from Greenland and are in coincidence with the lower air parcels during only the last ten hours of the trajectories (see Figure 6a). The layer above 22.5 km shows no HNO_3 depletion. It is thus very unlikely that particles formed in these air parcels. This is why calculations were started at the 22.5 km level.

4.3.4. Heterogeneous Chemistry

[44] The chemical code includes a detailed set of heterogeneous reactions relevant for chlorine activation. HCl depletion in the gas phase is specifically linked to the heterogeneous reactions of HCl with $ClONO_2$ and HOCl. Uptake coefficients for these reactions are calculated from the 2006 JPL data evaluation [*Sander et al.*, 2006]. The model of *Shi et al.* [2001] was used to calculate uptake coefficients on the surface of sulphate aerosols (the code is available at http://www.aerodyne.com/cacc/ClNO3-Kinetics.pdf).

[45] One of the remaining questions about heterogeneous chemistry in the polar stratosphere is linked to the loss of chemical species on STS particle surfaces. Laboratory measurements were carried out on mixtures of H_2SO_4 and H_2O particles. The presence of HNO_3 in PSC droplets could decrease reaction rates upon these surfaces; thus, models are thought to overestimate HCl destruction upon STS [*Drdla and Browell*, 2004; *Lowe and MacKenzie*, 2008].

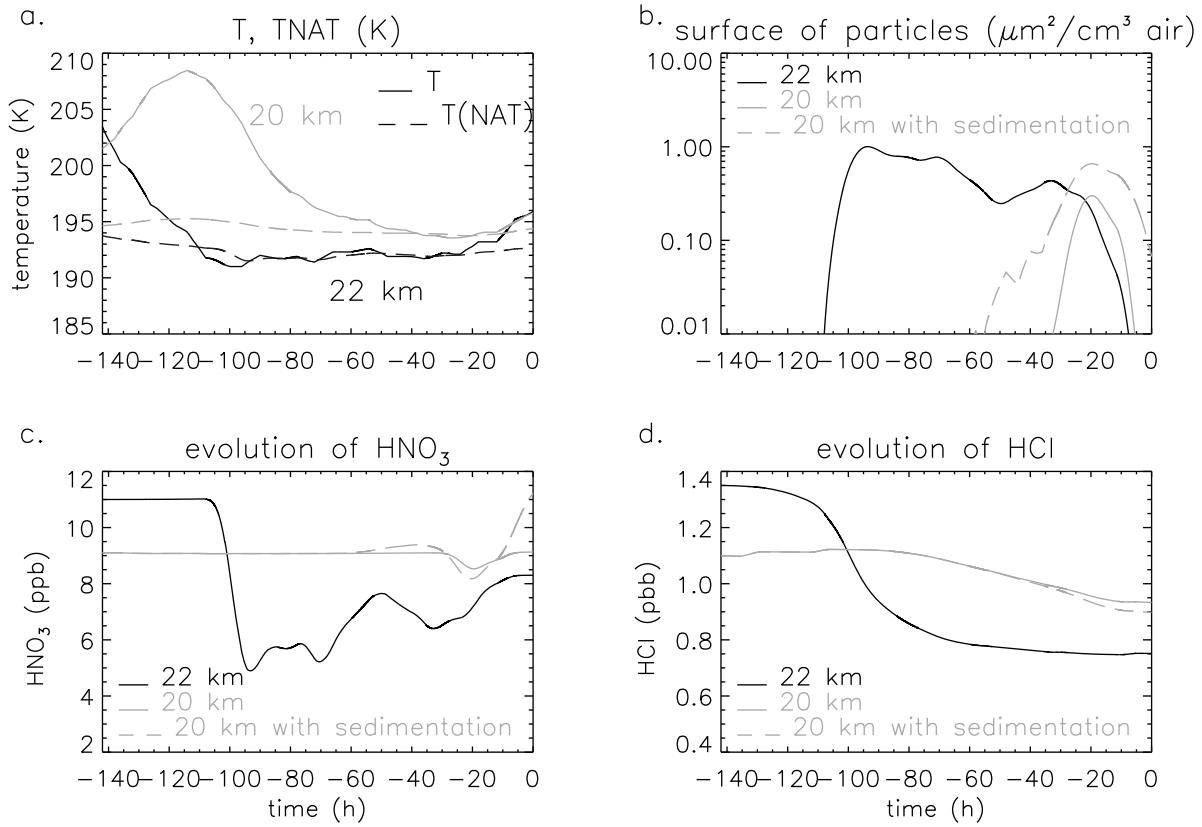

Figure 9. Model results with $J = 10^7$ cm^{-3} s^{-1} along the trajectories at 22 km (black) and 20 km (shaded). (a) Evolution of temperature T, after shift (i.e., $T = T_{ECMWF} + \Delta T$; see Table 1). The dash dotted curves show the threshold temperature for NAT formation, (b) Evolution of surface of NAT particles along these trajectories. The solid curves show the result without sedimentation; dashed curve with sedimentation at 20 km. (c) Evolution of HNO_3 mixing ratio, same convention as Figure 9b. (d) Evolution of HCl mixing ratio, same convention as Figures 9b and 9c.

4.4. Results

[46] The temperature measured in situ by the SPIRALE instrument is lower at all levels than the temperature predicted by either trajectory model (more than 2 K at 20–21 km, see section 4.1). In our study, temperatures below T_{NAT} are never reached along the trajectories with either model (HYSPLIT or Knudsen code). NAD and NAT nucleation rates become efficient when the temperature is 3 K–4 K below T_{NAT}. The temperature is really a sensitive parameter setting a threshold to initiate PSC formation. To perform the simulations we choose the trajectories calculated using ECMWF analyses where temperatures are the lowest and apply negative temperature shifts along the trajectories. We have tested different shifts on the temperature evolution along the trajectories every −0.05 K to a minimum value of −8 K (corresponding to a temperature below T_{ice}). Such large temperature shifts were used only as a sensitivity test. We then analyzed results obtained in terms of microphysical and chemical parameters: PSC altitude range, particle concentration, particle mean radius, and HNO_3 and HCl volume mixing ratio profiles. These systematic tests on temperature shifts along the trajectories have been performed for each NAT nucleation rate considered. The same type of temperature shift along trajectories has been used previously by *Santee et al.* [2002] to interpret and fit satellite data from Polar Ozone and Aerosol Measurement (POAM) and MLS instruments. Note that this shift depends on the altitude considered: The constraint is to nucleate solid particles and initiate their sedimentation.

4.4.1. Parameterization Tests

[47] Table 1 and Figure 8 summarize the main characteristics of the best results obtained using each parameterization in terms of temperature shift, microphysical, and chemical results.

[48] Concerning microphysical results, using *Salcedo et al.* [2001] and *Tabazadeh et al.* [2002] nucleation rates, it is necessary to apply temperature shifts as large as −7 K and −6.5 K on trajectories (from the ECMWF analysis) between 22 km to 20.5 km to nucleate NAT. This shift implies of course that the assumed temperature profile is lower not only than the ECMWF temperatures, but also lower than the observed one. The assumed profiles are shown in Figure 8c. The results for the parameterization of *Salcedo et al.* [2001] are similar with slightly lower temperature and therefore not shown. This profile is not in agreement with in situ temperature measurements by the payload. With our simulation, large particles (between 5 and 10 μm) are formed at 22 km and partially sedimented. For the time of the measurements a small concentration of

Table 1. Results Obtained as a Function of Considered Parameterization

Nucleation Parameter	*Salcedo et al.* [2001]	*Tabazadeh et al.* [2002]	Constant J $10^5 cm^{-3}$ s^{-1}	Constant J $10^7 cm^{-3}$ s^{-1}	Constant J $10^9 cm^{-3}$ s^{-1}	Observations
			ΔT[a]			
Max	−7 K	−6.5 K	−3.5 K	−3.8 K	−2 K	−2.2 K
Mean	−3.8 K	−3.6 K	–	−2.0 K	–	−1.3 K
			PSC[b]			
Altitude	All altitudes <22.5 km	All altitudes <22.5 km	20.5 km	20.5 km	–[c]	20 km
Concentration	concentration much too low $\sim 10^{-4} cm^{-3}$	concentration much too low $\sim 10^{-4} cm^{-3}$	$\sim 10^{-2} cm^{-3}$	$\sim 10^{-2} cm^{-3}$	–[c]	–
Mean radius	5 to 10 μm	5 to 10 μm	3 μm	1 μm	–[c]	0.5 to 1μm
			Species			
HNO_3	Correct denitrification, no renitrification		Correct denitrification, renitrification at 20 km		Incorrect fit	Denitrification at 20.5–22.5 km Renitrification 18.5–20.5 km
HCl	Correct fit in the 20.5–22.5 km range, overestimation below		Correct fit in the 20.5–22.5 km range, overestimation below		Incorrect fit	Depletion at 18–23 km

[a] ΔT is the shift imposed on the European Centre for Medium-Range Weather Forecasts (ECMWF) data (i.e., $T_{model} = T_{ECMWF} + \Delta T$). The ΔT_{mean} is the mean shift between 18 and 23 km, while ΔT_{max} is the maximum shift. The ΔT associated with observations corresponds to the difference between in situ measurements and ECMWF data.
[b] Polar stratospheric cloud.
[c] No sedimentation, too many particles.

NAT particles, less than that detected by the STAC aerosol counter, is predicted throughout the entire layer from 20 km to 22 km. In the PSC layer, the mean radius predicted is too large (5–10 μm) whereas STAC observations indicate particles with 0.5–1 μm radii. The *Mölher et al.* [2006] nucleation rate parameterization does even worse: No PSC particles are formed above T_{ice}. Our simulation results are in agreement with these authors' conclusion; their experimental results do not show nucleation rates necessary to fit observations in the polar stratosphere.

[49] The best simulations in terms of microphysical results are clearly obtained with the simplest parameterization, namely with a constant nucleation rates J of 10^5 and 10^7 cm^{-3} s^{-1}. The nucleation of particles was induced with a maximum temperature shift of −3.5 K and −3.8 K, respectively. It is worth noting that compared with the in situ measurements the temperature difference is not more than 2 K. Different J values (see Table 1) appear to simulate correctly the presence of a thin PSC at 20.5 km and its concentration. The values $J = 10^5$ and 10^7 cm^{-3} s^{-1} give quite similar results, with the only difference being the rate of growth. The best results are obtained using a NAT nucleation rate of 10^7 cm^{-3} s^{-1}, for which the predicted mean radius of particles better matches the STAC measurements. The simulation for this case is also shown in Figure 8.

[50] For chemical results associated with the simulated PSC it appears that if NAT particles are formed, HNO_3 is depleted from the gas phase in the layer 21–22.5 km. The renitrified layer highlighted by tracer-tracer correlations is reproduced only using a constant nucleation rate, although the simulated HNO_3 mixing ratio is larger than the measured one (Figure 8a). Using the *Tabazadeh et al.* [2002] J rate, the HNO_3 mixing ratio below 21.5 km does not differ from the initialization.

[51] Whichever nucleation parameterization is used, the HCl loss is simulated over the entire layer from 22 to 18 km (Figure 8b.). HCl is largely depleted above 19.5 km compared with the initial profile considered, but the intensity of the depletion is not reproduced at each level. The HCl depletion is more severe in the observations. However as the campaign was made at the end of January, and even if the 2005–2006 winter was not very cold, a previous activation of chlorine is highly probable. Thus our modeled initial HCl profile could be too high in some layers. Structures observed by the SPIRALE instrument are too thin (200m) to be simulated due to the vertical resolution used (500m) in the model.

4.4.2. Detailed Analysis Along Trajectories

[52] To characterize in detail the best simulations obtained in terms of temperature, microphysical, and chemical results, we present in Figure 9 the time evolution of the temperature, the NAT particles surface area along the trajectory, as well as the HNO_3 and HCl abundances at 22 km (inside the denitrified layer) and at 20 km (PSC layer). The equilibrium temperature of NAT with nitric acid and water vapor (dash dotted) is also presented in Figure 9a. Note that this figure does not show the temperature evolution of the ECMWF temperature directly, but shows the T_{ECMWF} shift (i.e., $T = T_{ECMWF} + \Delta T$; see Table 1), which is −3.6 K at 20 km. It shows the temperature taken as input by the model MIPLASMO for this run. Thus, the temperature has the same behavior as that shown in Figure 6, but is lower.

[53] Along the trajectory at 22 km, the threshold for NAT nucleation is first encountered 108 h before the measurements and NAT particle nucleation appears when the temperature reaches 192 K. Then 100 h before the measurements the temperature starts to increase. The number density and the NAT particle surface area decrease slowly. NAT particle nucleation occurring 108 h before the measurements leads to a strong decrease in the HNO_3 mixing ratio (11 ppbv to 4.25 ppbv). At 20 h before the measurements, the temperature increases strongly and all particles evaporate completely. The effect of particle sedimentation in this layer can be seen by looking at the time evolution of the HNO_3 mixing ratio (Figure 9c, black curve). As particles evaporate the HNO_3 mixing ratio increases, but at the time of the measurements when all particles have evaporated the

initial HNO_3 level is not recovered. This is due to particle sedimentation to lower levels. At this 22 km level an irreversible partial denitrification has occurred. The impact of chlorine activation on PSC particles leads to the irreversible HCl removal, which does not depend on particle sedimentation.

[54] To evaluate the impact of sedimentation on denitrification and renitrification processes, we performed two types of simulations. The first one considers in each layer a source of particles brought from higher altitudes and a loss of particles to lower altitudes by sedimentation (case with sedimentation shown with shaded dashed curve in Figure 9). The second type of simulation considers only the loss of particles to lower levels but no source from above (case without sedimentation with shaded solid curve in Figure 9). In the layer where the PSC was detected (20 km), the temperature falls below T_{NAT} between roughly −35 and −20 h before the measurements and nucleation of particles takes place. The effect of sedimentation from higher levels can be seen very clearly on the predicted NAT particle surface area in the 20 km layer (Figure 9b). When sedimentation from higher levels is not taken into account, small particles are formed at that time. They are too small to sediment. So at the very end of trajectories, when T increases, the particles evaporate and render the HNO_3: There was a temporary denitrification. No NAT particles are predicted at the time of the measurements. In the case sedimentation from higher levels is taken into account, the particles falling from the upper levels can reach the layer 55 h before the measurements but grow only when $T < T_{NAT}$ (−35 h to −20 h). Before and after this time, they evaporate in this layer and release HNO_3, which explains the small increase in HNO_3 between −55 and −35 h, and the large increase after −20 h. Some particles still remain at the time of the SPIRALE and STAC measurements. By comparison, when no sedimentation from the upper layers is taken into account, no HNO_3 increase is observed. The HCl profile (Figure 9d) also shows a small difference if particles are brought from higher altitudes. HCl is removed due to heterogeneous chemistry and this removal is slightly greater if the sedimentation process is taken into account, resulting in a larger surface area for heterogeneous reactions.

4.4.3. Discussion

[55] Tests using several nucleation rates available in the literature have been performed using a spectral microphysical model coupled to chemical code. Whichever nucleation rate is considered, it is necessary to apply a temperature shift along the trajectories to form PSC particles. The best result with respect to microphysical and chemical properties of the sampled air parcels is obtained using a constant nucleation rate of 10^7 cm^{-3} s^{-1}. This is consistent with previous model studies by *Drdla et al.* [2003]. A compilation of different constant nucleation rates from different studies can be found also in the review by *Lowe and MacKenzie* [2008]. Values between 2.9×10^{-6} and 25×10^{-6} cm^{-3} h^{-1} in air volume were found to fit well with observations made during several winters. In our simulation, the value of the number nucleation rate of 10^7 cm^{-3} s^{-1} in liquid phase corresponds approximately to a volume nucleation rate of 3×10^{-3} cm^{-3} h^{-1} in air. Thus, our value appears to be larger than the values summarized in the *Lowe and MacKenzie* [2008] review.

[56] Our study deals with a very specific case of PSC formation at high temperature very close to the NAT equilibrium temperature, whereas in the *Drdla et al.* [2003] study (winter 1999–2000) lower temperature conditions were encountered. These authors found that heterogeneous processes leading to NAT formation could explain the PSC observed during winter 1999–2000 as well as homogeneous ones. As homogeneous nucleation rates based on laboratory measurements often fail to explain the processes observed during polar winters, there is a debate to determine if the nucleation of NAT could be due to a heterogeneous mechanism rather than a homogeneous one [*Lowe and MacKenzie*, 2008]. In our case study, homogeneous processes do not seem to explain this PSC event. Although we cannot make a definite conclusion based on a single measurement case, our results seem to agree with the conclusion of *Lowe and MacKenzie* [2008]. Heterogeneous nucleation may explain the formation of particles in this particularly warm polar stratosphere.

[57] New observations could improve our understanding of NAT formation. For example, recent results from the Cloud-Aerosol Lidar and Infrared Pathfinder Satellite Observations (CALIPSO) spacecraft distinguished tenuous PSC mixtures containing low NAT number densities. Such mixtures were observed particularly in the low Antarctic stratosphere when the temperature was close to T_{NAT} [*Pitts et al.*, 2009].

5. Conclusion

[58] The polar campaign involving the SPIRALE balloon-borne instrument with the STAC instrument at Kiruna in January 2006 enabled us to measure simultaneously vertical profiles of O_3, N_2O, HNO_3, and HCl mixing ratios and aerosols, with a very high vertical resolution of a few meters. Characteristic features of depletion linked to PSC formation were observed on the HCl and HNO_3 profiles. Correlation curves of N_2O:HNO_3 and O_3:HNO_3 have been calculated from the in situ measurements. The detailed analysis of these correlations enables us to characterize denitrification and renitrification layers at a small scale. The denitrification occurred from 22.5 km to 20.5 km. HCl depletion covers a larger layer from 17 to 22.5 km. The STAC instrument observed a thin layer of PSCs located at 20 km, below the HNO_3 depleted layer.

[59] A possible explanation of the observations is that PSCs were formed in the 22 km layer, depleting HNO_3 by condensation during their growth. Then sedimentation of particles occurred, leading to denitrification and at the time of measurement particles were observed at 20 km. At the time the measurements were made the temperature was increasing and the PSC at 22 km had evaporated. Thus, only a filament of PSC was detected at 20 km.

[60] Model investigations have been conducted to interpret such complex vertical structures. Using a coupled microphysical and chemical model, runs were carried out in order to test nucleation, growth, and sedimentation processes of PSC particles simultaneously with adsorption of HCl and denitrification and renitrification mechanisms. Air parcel histories were determined using two trajectory codes driven by different meteorological datasets. In terms of air parcel location, both calculations are in agreement but the

temperature histories are different. The temperatures calculated with the *Knudsen et al.* [2001] and ECMWF data are lower than those calculated with the HYSPLIT model and the NCEP GDAS data. The temperatures measured by the payload are lower than those deduced from the trajectory calculations whichever data are used. We performed tests on the temperature along the trajectory required to initiate the nucleation of NAT particles in the denitrified layers. These tests have been made for several NAT nucleation rates discussed in the scientific literature [*Salcedo et al.*, 2001; *Tabazadeh et al.*, 2002; *Möhler et al.*, 2006]. The best results however were obtained using a constant nucleation rate of $J = 10^7$ cm^{-3} s^{-1}. In this case the model predictions are consistent with the hypothesis of sedimentation of particles previously nucleated in the 22.5–20.5 km range, leading to a local denitrification at 22 km and a renitrification at 20 km. This value found for the NAT nucleation rate is in agreement with the study by *Drdla et al.* [2003], but is above the usual constant nucleation rates used in other studies [*Lowe and MacKenzie*, 2008]. Heterogeneous nucleation, as previously discussed by *Lowe and MacKenzie* [2008], may explain our observations. These results suggest that further investigations are still needed to settle the debate on the formation of NAT and NAD particles in the Arctic region regardless of polar stratosphere conditions, whether cold as in the study by *Drdla et al.* [2003] or warm as in our study.

[61] **Acknowledgments.** The SPIRALE instrument was launched in the context of the Envisat validation project funded by ESA and CNES. We thank G. Moreau for fruitful discussion. We deeply thank L. Pomathiod, M. Chartier, G. Jannet, T. Vincent (LPC2E) and the CNES launching balloon team for successful operations. We gratefully acknowledge the NOAA Air Resources Laboratory for the provision of the HYSPLIT transport and dispersion model and the READY website (http://www.arl.noaa.gov/ready.html) used in this publication. We acknowledge N. Larsen and B. Knudsen from the Danish Meteorological Institute for the PSC microphysical code and the isentropic trajectories code they provided at the beginning of the MiPlaSMO model development. We also thank Franck Lefèvre for the management of the REPROBUS CTM and Alain Hauchecorne for the potential vorticity calculations from the Mimosa Model. We finally thank the three anonymous reviewers for their helpful comments, which have markedly improved our paper.

References

Bemer, D., J. F. Fabries, and A. Renoux (1990), Calculation of the theoretical response of an optical particle counter and its practical usefulness, *J. Aerosol Sci.*, *21*, 689–700, doi:10.1016/0021-8502(90)90123-F.

Berthet, G., et al. (2006), On the ability of chemical transport models to simulate the vertical structure of the N_2O, NO_2, and HNO_3 species in the mid-latitude stratosphere, *Atmos. Chem. Phys.*, *6*, 1599–1609, doi:10.5194/acp-6-1599-2006.

Berthet, G., et al. (2007), Remote-sensing measurements in the polar vortex: Comparison to in situ observations and implications for the simultaneous retrievals and analysis of the NO_2 and OClO species, *J. Geophys. Res.*, *112*, D21310, doi:10.1029/2007JD008699.

Bertram, A. K., and J. J. Sloan (1998), The nucleation rate constants and freezing mechanism of nitric acid trihydrate aerosol under stratospheric conditions, *J. Geophys. Res.*, *103*, 13,261–13,265, doi:10.1029/98JD00921.

Bregman, A., et al. (1995), Aircraft measurements of O_3, HNO_3 and N_2O in the winter Arctic lower stratosphere during the Stratosphere-Troposphere Experiment by Aircraft Measurements (STREAM) 1, *J. Geophys. Res.*, *100*, 11,245–11,260, doi:10.1029/95JD00219.

Brogniez, C., et al. (2003), Polar stratospheric cloud microphysical properties measured by the microRADIBAL instrument on 25 January 2000 above Esrange and modeling interpretation, *J. Geophys. Res.*, *108*(D6), 8332, doi:10.1029/2001JD001017.

Carslaw, K. S., J. A. Kettleborough, M. J. Northway, S. Davies, R. S. Gao, D. W. Fahey, D. G. Baumgardner, M. P. Chipperfield, and A. Kleinböhl (2002), A vortex simulation of the growth and sedimentation of large nitric acid hydrate particles, *J. Geophys. Res.*, *107*(D20), 8300, doi:10.1029/2001JD000467.

Cortesi, U., et al. (2007), Geophysical validation of MIPAS-Envisat operational ozone data, *Atmos. Chem. Phys.*, *7*, 4807–4867, doi:10.5194/acpd-7-5805-2007.

Davies, S., G. W. Mann, K. S. Carslaw, M. P. Chipperfield, J. J. Remedios, G. Allen, A. M. Waterfall, R. Spang, and G. C. Toon (2006), Testing our understanding of Arctic denitrification using MIPAS-E satellite measurements in winter 2002/2003, *Atmos. Chem. Phys.*, *6*, 3149–3161, doi:10.5194/acp-6-3149-2006.

Deshler, T., et al. (2003), Large nitric acid particles at the top of an Arctic stratospheric cloud, *J. Geophys. Res.*, *108*(D16), 4517, doi:10.1029/2003JD003479.

Dibb, J. E., E. Scheuer, M. Avery, J. Plant, and G. Sachse (2006), In situ evidence for renitrification in the Arctic lower stratosphere during the polar aura validation experiment (PAVE), *Geophys. Res. Lett.*, *33*, L12815, doi:10.1029/2006GL026243.

Douglass, A. R., M. R. Schoeberl, R. S. Stolarski, J. W. Waters, J. M. Russell III, A. E. Roche, and S. T. Massie (1995), Interhemispheric differences in springtime production of HCl and $ClONO_2$ in the polar vortices, *J. Geophys. Res.*, *100*, 13,967–13,978, doi:10.1029/95JD00698.

Dörnbrack, A., and M. Leutbecher (2001), Relevance of mountain waves for the formation of polar stratospheric clouds over Scandinavia: A 20 year climatology, *J. Geophys. Res.*, *106*, 1583–1593, doi:10.1029/2000JD900250.

Drdla, K., M. R. Schoeberl, and E. V. Browell (2003), Microphysical modeling of the 1999–2000 Arctic winter: 1. Polar stratospheric clouds, denitrification, and dehydration, *J. Geophys. Res.*, *108*(D5), 8312, doi:10.1029/2001JD000782.

Draxler, R. R., and G. D. Rolph (2003), HYSPLIT (Hybrid Single-Particle Lagrangian Integrated Trajectory) Model, NOAA Air Resources Laboratory, Silver Spring, Md.

Drdla, K., and E. V. Browell (2004), Microphysical modeling of the 1999-2000 Arctic winter: 3. Impact of homogeneous freezing on polar stratospheric clouds, *J. Geophys. Res.*, *109*, D10201, doi:10.1029/2003JD004352.

Engel, A., et al. (2006), On the observation of mesospheric air inside the arctic stratospheric polar vortex in early 2003, *Atmos. Chem. Phys.*, *6*, 267–282.

Fahey, D. W., et al. (2001), The detection of large HNO_3-containing particles in the winter arctic stratosphere, *Science*, *291*, 1026–1031.

Gobiet, A. A., U. Foelsche, A. K. Steiner, M. Borsche, G. Kirchengast, and J. Wickert (2005), Climatological validation of stratospheric temperatures in ECMWF operational analyses with CHAMP radio occultation data, *Geophys. Res. Lett.*, *32*, L12806, doi:10.1029/2005GL022617

Grooß, J.-U., G. Günther, R. Müller, P. Konopka, H. Schlager, C. Voigt, C. M. Olk, and G. C. Toon (2005), Simulation of denitrification and ozone loss for the Arctic winter 2002/2003, *Atmos. Chem. Phys.*, *5*, 1437–1448, doi:10.5194/acp-5-1437-2005.

Hauchecorne, A., S. Godin, M. Marchand, B. Heese, and C. Souprayе (2002), Quantification of the transport of chemical constituents from the polar vortex to midlatitudes in the lower stratosphere using the high-resolution advection model MIMOSA and effective diffusivity, *J. Geophys. Res.*, *107*(D20), 8289, doi:10.1029/2001JD000491.

Huret, N., M. Pirre, A. Hauchecorne, C. Robert, and V. Catoire (2006), On the vertical structure of the stratosphere at midlatitudes during the first stage of the polar vortex formation and in the polar region in the presence of a large mesospheric descent, *J. Geophys. Res.*, *11*, D06111, doi:10.1029/2005JD006102.

Kleinböhl, A., H. Bremer, H. Küllmann, J. Kuttippurath, E. V. Browell, T. Canty, R. J. Salawitch, G. C. Toon, and J. Notholt (2005), Denitrification in the Arctic mid-winter 2004/2005 observed by airborne submillimeter radiometry, *Geophys. Res. Lett.*, *32*, L19811, doi:10.1029/2005GL023408.

Knopf, D. A., T. Koop, B. P. Luo, U. G. Weers, and T. Peter (2002), Homogeneous nucleation of NAD and NAT in liquid stratospheric aerosols: Insufficient to explain denitrification, *Atmos. Chem. Phys.*, *2*, 207–214.

Knudsen, B. M., J. P. Pommereau, A. Garnier, M. Nunez-Pinharanda, L. Denis, G. Letrenne, M. Durand, and J. M. Rosen (2001), Comparison of stratopheric air parcel trajectories based on different meteorological analyses, *J. Geophys. Res.*, *106*, 3415–3424, doi:10.1029/2000JD900608.

Knudsen, B. M., T. Christensen, A. Hertzog, A. Deme, F. Vial, and J.-P. Pommereau (2006), Accuracy of analyzed temperatures, winds and trajectories in the Southern Hemisphere tropical and midlatitude stratosphere as compared to long-duration balloon flights, *Atmos. Chem. Phys.*, *6*, 5391–5397, doi:10.5194/acp-6-5391-2006.

Larsen, N., et al. (2002), Microphysical mesoscale simulations of polar stratospheric cloud formation constrained by in situ measurements of chemical and optical cloud properties, *J. Geophys. Res.*, *107*(D20), 8301, doi:10.1029/2001JD000999.

Larsen, N., et al. (2004), Formation of solid particles in synoptic-scale Arctic PSCs in early winter 2002/2003, *Atmos. Chem. Phys.*, *4*, 2001–2013, doi:10.5194/acp-4-2001-2004.

Lefèvre, F., F. Figarol, K. S. Carslaw, and T. Peter (1998), The 1997 Arctic ozone depletion quantified from three-dimensional model simulations, *Geophys. Res. Lett.*, *25*, 2425–2428.

Lowe, D., A. R. MacKenzie, H. Schlager, C. Voigt, A. Dörnbrack, M. J. Mahoney, and F. Cairo (2006), Liquid particle composition and heterogeneous reactions in a mountain wave polar stratospheric cloud, *Atmos. Chem. Phys.*, *6*, 3611–3623, doi:10.5194/acpd-5-9547-2005.

Lowe, D., and A. R. MacKenzie (2008), Polar stratospheric cloud microphysics and chemistry, *J. Atmos. Sol. Terr. Phys.*, *70*, 13–40, doi:10.1016/j.jastp.2007.09.011.

Mahieu, E., et al. (2008), Validation of ACE-FTS v2.2 measurements of HCl, HF, CCl_3F and CCl_2F_2 using space-, balloon- and ground-based instrument observations, *Atmos. Chem. Phys.*, *8*, 6199–6221.

Manney, G. L., H. A. Michelsen, M. L. Santee, M. R. Gunson, F. W. Irion, A. E. Roche, and N. J. Livesey (1999), Polar vortex dynamics during spring and fall diagnosed using trace gas observations from the Atmospheric Trace Molecule Spectroscopy instrument, *J. Geophys. Res.*, *104*, 18,841–18,866, doi:10.1029/1999JD900317.

Manney, G. L., et al. (2008), The evolution of the stratopause during the 2006 major warming: Satellite data and assimilated meteorological analyses, *J. Geophys. Res.*, *113*, D11115, doi:10.1029/2007JD009097.

Mébarki, Y., V. Catoire, N. Huret, G. Berthet, C. Robert, and G. Poulet (2010), More evidence for very short-lived substance contribution to stratospheric chlorine inferred from HCl balloon-borne in situ measurements in the tropics, *Atmos. Chem. Phys.*, *10*, 1–13, doi:10.5194/acp-10-397-2010.

Michelsen, H. A., G. L. Manney, M. R. Gunson, and R. Zander (1998), Correlations of stratospheric abundances of NOy, O_3, N_2O, and CH_4 derived from ATMOS measurements, *J. Geophys. Res.*, *103*, 28,347–28,359.

Mölher, O., H. Bunz, and O. Stetzer (2006), Homogeneous nucleation rates of nitric acid dihydrate (NAD) at simulated stratospheric conditions–Part II: Modeling, *Atmos. Chem. Phys.*, *6*, 3035–3047.

Montoux, N., et al. (2009), Evaluation of balloon and satellite water vapor measurements in the Southern tropical and subtropical UTLS during the HIBISCUS campaign, *Atmos. Chem. Phys.*, *9*, 5299–5319.

Moreau, G., C. Robert, V. Catoire, M. Chartier, C. Camy-Peyret, N. Huret, M. Pirre, L. Pomathiod, and G. Chalumeau (2005), SPIRALE: A multispecies in situ balloon-borne instrument with six tunable diode laser spectrometers, *Appl. Opt.*, *4*, 5972–5989, doi:10.1364/AO.44.005972.

Müller, R., et al. (2007), Impact of mesospheric intrusions on ozone-tracer relations in the stratospheric polar vortex, *J. Geophys. Res.*, *112*, D23307, doi:10.1029/2006JD008315.

Nassar, R., et al. (2006), A global inventory of stratospheric chlorine in 2004, *J. Geophys. Res.*, *111*, D22312, doi:10.1029/2006JD007073.

Newman, P. A., et al. (2002), An overview of the SOLVE/THESEO 2000 campaign, *J. Geophys. Res.*, *107*(D20), 8259, doi:10.1029/2001JD001303.

Northway, M. J., et al. (2002), An analysis of large HNO_3-containing particles sampled in the Arctic stratosphere during the winter of 1999/2000, *J. Geophys. Res.*, *107*(D20), 8298, doi:10.1029/2001JD001079.

Ovarlez, J., and H. Ovarlez (1995), Water vapor and aerosol measurements during SESAME, and the observation of low water vapor content layers, *Air Pollution Rep. 56, Polar Stratospheric Ozone*, Proceedings of the third European Workshop, Commission of the European Communities, Brussels, Belgium.

Pitts, M. C., L. R. Poole, and L. W. Thomason (2009), CALIPSO polar stratospheric cloud observations: Second-generation detection algorithm and composition discrimination, *Atmos. Chem. Phys.*, *9*, 7577–7589, doi:10.5194/acpd-9-8121-2009.

Renard, J. B., J. Ovarlez, G. Berthet, D. Fussen, F. Vanhellemont, C. Brogniez, E. Hadamcik, M. Chartier, and H. Ovarlez (2005), Optical and physical properties of stratospheric aerosols from balloon measurements in the visible and near-infrared domains; III. Presence of aerosols in the middle stratosphere, *Appl. Opt.*, *44*, 4086–4095.

Renard, J.-B., et al. (2008), Validation of GOMOS-Envisat vertical profiles of O_3, NO_2, NO_3, and aerosol extinction using balloon-borne instruments and analysis of the retrievals, *J. Geophys. Res.*, *113*, A02302, doi:10.1029/2007JA012345.

Ricaud, P., et al. (2005), Polar vortex evolution during the 2002 Antarctic major warming as observed by the Odin satellite, *J. Geophys. Res.*, *110*, D05302, doi:10.1029/2004JD005018.

Rivière, E. D., et al. (2000), Role of lee waves in the formation of solid polar stratospheric clouds: Case studies from February 1997, *J. Geophys. Res.*, *105*, 6845–6853, 10.1029/1999JD900908.

Rivière, E. D., Y. Terao, and H. Nakajima (2003), A Lagrangian method to study stratospheric nitric acid variations in the polar regions as measured by the Improved Limb Atmospheric Spectrometer, *J. Geophys. Res.*, *108* (D23), 4718, doi:10.1029/2003JD003718.

Rothman, L. S., et al. (2005), The HITRAN 2004 molecular spectroscopic database, *J. Quant. Spectrosc. Radiat. Transfer*, *96*, 139–204, doi:10.1016/j.jqsrt.2004.10.008.

Russell, P. B., et al. (1996), Global to microscale evolution of the Pinatubo volcanic aerosol derived from diverse measurements and analyses, *J. Geophys. Res.*, *101*, 18,745–18,763, doi:10.1029/96JD01162.

Salcedo, D., L. T. Molina, and M. J. Molina (2001), Homogeneous freezing of concentrated aqueous nitric acid solutions at polar stratospheric temperatures, *J. Phys. Chem. A.*, *105*, 1433–1439.

Sander, S. P., et al. (2006), Chemical kinetics and photochemical data for use in atmospheric studies: Evaluation 15, *Rep. 06-02*, Jet Propulsion Laboratory, Pasadena, Ca.

Santee, M. L., A. Tabazadeh, G. L. Manney, M. D. Fromm, R. M. Bevilacqua, J. W. Waters, and E. J. Jensen (2002), A Lagrangian approach to studying Arctic polar stratospheric clouds using UARS MLS HNO3 and POAM II aerosol extinction measurements, *J. Geophys. Res.*, *107*(D10), 4098, doi:10.1029/2000JD000227.

Santee, M. L., et al. (2008), A study of stratospheric chlorine partitioning based on new satellite measurements and modeling, *J. Geophys. Res.*, *113*, D12307, doi:10.1029/2007JD009057.

Schoeberl, M. R., et al. (2006), Chemical observations of a polar vortex intrusion, *J. Geophys. Res.*, *111*, D20306, doi:10.1029/2006JD007134.

Shi, Q., J. T. Jayne, C. E. Kolb, D. R. Worsnop, and P. Davidovits (2001), Kinetic model for reaction of $ClONO_2$ with H_2O and HCl and HOCl with HCl in sulfuric acid solutions, *J. Geophys. Res.*, *106*, 24,259–24,274, doi:10.1029/2000JD000181.

Solomon, S. (1999), Stratospheric ozone depletion: A review of concepts and history, *Rev. Geophys.*, *37*, 275–316, doi:10.1029/1999RG900008.

SPARC (2006), Assessment of stratospheric aerosols properties (ASAP), *SPARC Rep. No. 4* Stratospheric Processes and their Role in Climate, Geneva, Switzerland.

Stetzer, O., O. Möhler, R. Wagner, S. Benz, H. Saathoff, H. Bunz, and O. Indris (2006), Homogeneous nucleation rates of nitric acid dihydrate (NAD) at simulated stratospheric conditions–Part I: Experimental results, *Atmos. Chem. Phys.*, *6*, 3023–3033.

Strong, K., et al. (2008), Validation of ACE-FTS N_2O measurements, *Atmos. Chem. Phys.*, *8*, 4759–4786, doi:10.5194/acp-8-4759-2008.

Tabazadeh, A., E. J. Jensen, O. B. Toon, K. Drdla, and M. R. Schoeberl (2001), Role of stratospheric polar freezing belt in denitrification, *Science*, *29*, 2591–2594, doi:10.1126/science.1057228.

Tabazadeh, A., Y. S. Djikaev, P. Hamill, and H. Reiss (2002), Laboratory evidence for surface nucleation of solid polar stratospheric cloud particles, *J. Phys. Chem.*, *106*, 10,238–10,246, doi:10.1021/jp021045k.

Urban, J., et al. (2005), Odin/SMR limb observations of stratospheric trace gases: Validation of N_2O, *J. Geophys. Res.*, *110*, D09301, doi:10.1029/2004JD005394.

Voigt, C., et al. (2000), Nitric acid trihydrate (NAT) in polar stratospheric clouds, *Science*, *290*, 1756–1758, doi:10.1126/science.290.5497.1756.

Wang, D. Y., et al. (2007), Validation of MIPAS HNO_3 operational data, *Atmos. Chem. Phys.*, *7*, 4905–4934, doi:10.5194/acp-7-4905-2007.

Wilmouth, D. M., R. M. Stimpfle, J. G. Anderson, J. W. Elkins, D. F. Hurst, R. J. Salawitch, and L. R. Lait (2006), Evolution of inorganic chlorine partitioning in the Arctic polar vortex, *J. Geophys. Res.*, *111*, D16308, doi:10.1029/2005JD006951.

WMO (2007), Scientific Assessment of Ozone Depletion, *Rep. 50*, World Meteorological Organization, Geneva, Switzerland.

Wolff, M. A., et al. (2008), Validation of HNO_3, $ClONO_2$, and N_2O_5 from the Atmospheric Chemistry Experiment Fourier Transform Spectrometer (ACE-FTS), *Atmos. Chem. Phys.*, *8*, 3529–3562, doi:10.5194/acp-8-3529-2008.

G. Berthet, V. Catoire, B. Gaubicher, N. Huret, J.-B. Renard, and C. Robert, Laboratoire de Physique et Chimie de l'Espace et de l'Environnement, CNRS-Université d'Orléans, UMR 6115, FR-45071, Orléans, Cedex 2, France.

A. Grossel, Institut National de la Recherche Agronomique, UR 0272, Science du Sol, Centre de Recherche d'Orléans, CS 40001 Ardon, FR-45075 Orléans, Cedex 2, France. (agnes.grossel@orleans.inra.fr)